Journal of Photochemistry & Photobiology, A: Chemistry 444 (2023) 114901

Contents lists available at ScienceDirect

Journal of Photochemistry & Photobiology, A: Chemistry

journal homepage: www.elsevier.com/locate/jphotochem

Contribution of CuO on lamellar $BiVO_4/Bi_2O_3$-based semiconductor for photoconversion of CO_2

Patricia Gon Corradini [a,b], Juliana Ferreira de Brito [a,c], Sirlon F Blaskievicz [a], Byanca S Salvati [a], Beatriz Costa e Silva Menezes [c], Maria Valnice Boldrin Zanoni [c], Lucia Helena Mascaro [a,*]

[a] Department of Chemistry, Federal University of São Carlos, Rod. Washington Luiz, Km 235, CEP 13565-905 São Carlo, SP, Brazil
[b] Fluminense Federal Institute of Education, Science and Technology, Campus Itaperuna, Itaperuna, RJ 28300-000, Brazil
[c] Institute of Chemistry - Araraquara, UNESP, Rua Francisco Degni, 55, Bairro Quitandinha, 14800-900 Araraquara, SP, Brazil

ARTICLE INFO

Keywords:
Photosynthesis
Cocatalyst
Fuel production
Global warming

ABSTRACT

Lamellar $BiVO_4$ is a photocatalyst recognized as an effective visible-light-driven semiconductor that is active in CO_2 reduction but faces challenges such as high recombination rate and low mobility of photogenerated charge carriers. Additionaly, Cu_XO are well-known materials for CO_2 photosynthesis, and Bi_2O_3 improves the generation of organic compounds from CO_2 reduction with more than one carbon. In this sense, this paper evaluates the influence of small amounts of copper oxide on lamellar $BiVO_4$-Bi_2O_3 prepared by a microwave-assisted route on the CO_2 photoreduction activity. Lamellar $BiVO_4$-Bi_2O_3 powder catalysts modified by different percentages of CuO were synthesized using microwave heating at 140 °C and 1200 rpm for 15 min. Electrochemical and photochemical characterizations showed that small amounts of copper, such as 1.0%, enhanced the absorption of visible light, improved charge transfer, mitigated charge recombination, and increased the yield of products (acetone and methanol). Furthermore, the flat band potential of the catalyst modified with 1.0% of copper was located at a more negative potential than the unmodified sample, which favored the photocatalytic reduction of the CO_2. As a result, the study achieved a 38-fold improvement in methanol generation (1373.5 μmol L^{-1} g_{cat}^{-1} and a 62% increase in acetone formation (12.5 μmol L^{-1} g_{cat}^{-1}) under UV–Vis light incidence over 2 h of reaction at ambient pressure and temperature, compared to pure $BiVO_4$ (36.3 μmol L^{-1} g_{cat}^{-1} of methanol and 7.7 μmol L^{-1} g_{cat}^{-1} of acetone).

1. Introduction

Human activity has been changing the concentration of heat-trapping compounds, such as carbon dioxide (CO_2), and changing the earth's climate [1]. Its high concentration in the atmosphere has been contributing to fueling greater demand for methods capable of promoting the reuse or the conversion of CO_2 [2,3]. To this end, among the diversity of strategies to reduce CO_2 into valuable chemicals and/or through high energy content fuel, the processes mimicking natural reactions such as artificial photosynthesis retain attention [4–6]. The idea of recycling CO_2 using light absorption comes from the observation of photosynthetic systems that absorbs CO_2 and light energy and convert them into organic molecules, as described by the chemical Eq. (1). Similarly, artificial reactions can be used to convert CO_2 into fuels. In this case, fuels can be produced directly from the dissociation of water into hydrogen, the reduction of CO_2 to $^{-}CO_2^{\bullet}$ and by these intermediates interaction, producing organic molecules with high energy content, as can be demonstrated by the chemical equations (2) to (6) for the methanol and acetone production from CO_2 photoreduction, for example [7–9].

$$6CO_2 + 6H_2O + h\nu \rightarrow C_6H_{12}O_6 + 6O_2 \quad (1)$$

$$H_2O + h_{VB}^{+} \rightarrow H^{+} + OH^{\bullet} \quad (2)$$

$$H^{+} + e_{CB}^{-} \rightarrow H^{\bullet} \quad (3)$$

$$CO_2 + e_{CB}^{-} \rightarrow CO_2^{\bullet -} \quad (4)$$

$$CO_2^{\bullet -} + 6H^{\bullet} \rightarrow CH_3OH + H_2O \quad (5)$$

$$CO_2^{\bullet -} + 2CH_3^{\bullet} + 1e^{-} + 2H^{+} \rightarrow CH_3COCH_3 + H_2O \quad (6)$$

* Corresponding author.
E-mail address: lmascaro@usfcar.br (L.H. Mascaro).

https://doi.org/10.1016/j.jphotochem.2023.114901
Received 17 February 2023; Received in revised form 5 May 2023; Accepted 30 May 2023
Available online 3 June 2023

Thus, the use of efficient semiconductor materials with the ability to photogenerate electron/hole pairs (h^+/e^-) is a crucial target in the photocatalytic process [2,4,10,11]. The far more employed p-type semiconductors for photochemical reduction of CO_2 are the copper-based catalysts [12–15], mainly in photocatalytic systems [8,16,17], due to their low toxicity, high abundance, and wide production distribution [18]. Besides that, the rate and selectivity of Cu and CuO_x catalysts are close to the ideal, and the Cu transition state energies are very close to the optimum transition state energies for the adsorption of carbon monoxide (CO) [19], beyond the good behavior of copper-based catalysts in the CO_2 reduction by photochemical reactions, this type of electrode presents low stability under irradiation [12,20]. This fact raised interest in a couple of Cu and Cu_xO with a variety of other materials, once common ways to avoid photocorrosion are (i) to develop protective layers and (ii) to separate and transmit the photogenerated electron-hole pair on time [21]. Looking at those options, there is some interest in a couple of metal and semiconductor oxides [22].

The extensive diversity of different semiconductors has been studied and employed in CO_2 reduction since the growth of this area at the beginning of 2010 [4]. Lamellar $BiVO_4$, an environmentally friendly material, presents nontoxic and abundant components, with good stability in aqueous media and a suitable band gap for visible light (around 2.4 eV for the monoclinic phase) [23,24], is a good example of photocatalysts recently investigated for CO_2 reduction reaction under photocatalysis technique [4,25,26]. Because of its lamellar structure, it presents an anisotropic distribution of the electron/hole pair photogenerated that favors reduction reactions such as CO_2 photosynthesis [27,28]. The Bi^{3+} sites can anchor reaction intermediates for the V sites further transferring the electrons for reduction [29,30].

However, this catalyst presents a weak reduction potential of the electrons in the conduction band (CB) and slow electron transfer dynamics, inhibiting photocatalytic performances and restricting its application [7]. The presence of bismuth oxide (Bi_2O_3) can help to improve $BiVO_4$ characteristics for CO_2 reduction. Many mechanisms of synthesis, such as the hydrothermal, microwave, and precipitation methods result in a co-formation of Bi_2O_3 in $BiVO_4$ synthesis [4,31,32]. When Bi_2O_3 is present in small amounts on $BiVO_4$, it facilitates the separation of charge carriers, enhances the diffusion of these charges on the semiconductor surface [33], and promotes the homolytic cleavage of methanol, ultimately contributing to the production of acetone [4].

Taking that into consideration, this work combined $BiVO_4$ lamellar semiconductor with Bi_2O_3 and CuO nanoparticles by microwave synthesis to be applied in the CO_2 reduction reaction by a photocatalysis approach.

2. Experimental section

2.1. Synthesis of Bi-based materials

The methodology of the $BiVO_4$ powder catalyst preparation is described by Brito and coworkers [26]. In brief, a solution of 0.536 g of bismuth (III) chloride ($BiCl_3$, Sigma-Aldrich®), 0.255 g of hexadecyltrimethylammonium bromide ($C_{19}H_{42}BrN$, Sigma-Aldrich®), and 0.340 g of sodium orthovanadate (Na_3VO_4, Sigma-Aldrich®) in 20 mL of ethylene glycol ($C_2H_6O_2$, Synth®) was prepared under magnetic stirring. The solution was transferred to a microwave system (Anton-Paar®) and heated from room temperature to 140 °C at a rate of 5 °C min^{-1} under constant 1200 rpm of magnetic stirring. The system was maintained at the desired temperature for 15 min before being allowed to cool down. For the Cu-$BiVO_4$ synthesis, copper chloride ($CuCl_2{\cdot}2H_2O$, Vetec®) was added to the reaction medium along with the $BiVO_4$ semiconductor precursors. The obtained product was then centrifuged with water and ethanol, filtered, and oven-dried at 50 °C for 12 h.

2.2. Physical characterization

The as-synthetized $BiVO_4$-Bi_2O_3/CuO catalysts were characterized by Scanning electron microscopy (SEM) using an FEI microscope, model Inspect F50; X-ray diffraction (XRD) obtained on a Siemens AXS Analytical X-Ray D 5005 diffractometer with scans between 10° and 80° at 2° min^{-1}. High-resolution transmission electron microscopy (HR-TEM) images were acquired on a JEM-2100F LaB6 (Joel) microscope operating at 200 kV. Raman spectroscopy was performed on a Micro Raman Horiba iHR 550 spectrophotometer with a 633 nm laser. UV–VIS Diffuse Reflectance Spectroscopy (DRS) was obtained on a Varian Model Cary 5G UV–vis-NIR spectrophotometer coupled with an integrating sphere with a wavelength range from 250 to 800 nm. The analysis of DRS spectra was performed by traditional methods, employing the Kubelka-Munk function and Tauc equation [34], to relate the energy of the incident photons and the energy of the band gap (Eg) of the material. X-ray photoelectron spectroscopy (XPS) was obtained on Scienta Omicron (model ESCA 2SR) spectrometer, with magnesium monochromator (Mg Kα), calibrated using the Carbon 1 s peak (284.8 eV).

2.3. Photoelectrochemical characterizations

The photocatalysts were deposited in gas diffusion layer carbon (GDL) by spin-coating. For that, 0.15 g of each powder catalyst was suspended in 1.27 mL ethanol with 0.01 mg ethylcellulose. After complete homogenization, 0.1 mL of this solution was deposited on the GDL surface at 300 rpm for 30 s. This procedure was repeated three times, forming three deposited layers, followed by thermal treatment at 180 °C for 30 min.

The obtained photoelectrodes were then evaluated in a typical three-electrode cell, with Na_2SO_4 0.5 mol L^{-1} (pH adjusted to 8.5) as the supporting electrolyte and constant nitrogen flux. The counter and the reference electrode were a Pt plate and Ag/AgCl in saturated KCl ($E^\circ_{Ag/AgCl} = +0.197$ V vs NHE – normal hydrogen electrode) respectively. For the conversion of measured potential versus Ag/AgCl reference ($E_{Ag/AgCl}$) to reversible hydrogen electrode (RHE) potential (E_{RHE}) the Nernst equation was employed:

$$E_{RHE} = E_{Ag/AgCl} + E^\circ_{Ag/AgCl} + (0.059 \times pH) \quad (6)$$

Electrochemical impedance spectroscopy (EIS) was conducted at the open circuit potential (OCP), scanning a frequency range of 10 kHz to 10 mHz with an amplitude of 10 mV. Mott-Schottky analysis was performed by measuring the impedance spectra of the samples in a potential range from 0.68 to 0.18 V RHE, 10 mV potential amplitude, and frequencies of 5 kHz to 1 kHz. Photocurrent measurements were performed with linear sweep voltammograms, measured at 10 mV s^{-1}, under pulsed illumination ($t_{on} = t_{off} = 1$ s) in the front side of the photoelectrode using a solar simulator (LCS-100 – Newport, with irradiance adjusted to 100 mW cm^{-2}) as the light source.

2.4. Photocatalytic reduction of CO_2

The CO_2 photoreduction methodology was widely described by Corradini et al. [4]. Briefly, the photocatalytic reduction of CO_2 was performed in an internal illumination reactor (using a Philips 125 W lamp, model HPL-N 1542) at a controlled temperature (5 °C) 0.2 g of the powder catalyst was suspended in 220 mL of 0.1 mol L^{-1} $NaHCO_3$ at pH 8.0, and magnetically stirred in the dark for 30 min before irradiation. Aliquots of 2.0 mL suspensions were collected and analyzed using gas chromatography with flame ionization detection (GC-FID) according to the methodology described in Brito et al. [35].

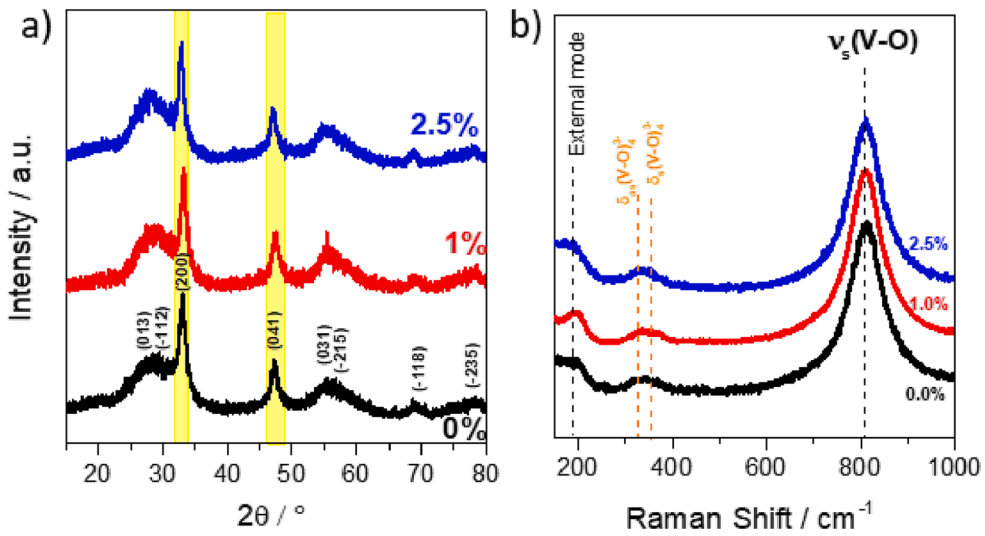

Fig. 1. A) XRD diffractograms and b) Raman spectra obtained for the $BiVO_4$-Bi_2O_3 photocatalyst modified with 0.0%, 1.0%, and 2.5% of copper.

Table 1
Crystallite size and band gap values of $BiVO_4$-Bi_2O_3 with and without CuO modification in different percentages.

Material	Crystallite size (nm)*	Band gap (eV)
$BiVO_4/Bi_2O_3$– 0.0%	6.0	2.94
$BiVO_4/Bi_2O_3$ – 1.0% Cu	6.5	3.17
$BiVO_4/Bi_2O_3$ – 2.5% Cu	7.4	3.27

*Sherry equation, arithmetic means of peaks in 33° and 48°.

3. Results and discussion

3.1. Physical characterization of $BiVO_4$-Bi_2O_3/CuO

Seeking an improvement in the $BiVO_4$-Bi_2O_3 photocatalytic activity for CO_2 reduction using the photocatalysis technique, the new semiconductor was synthesized in the presence of different quantities of copper precursor, forming the so-called $BiVO_4$-Bi_2O_3/CuO(1.0%) and $BiVO_4$-Bi_2O_3/CuO(2.5%). The amount of CuO was maintained in a low mass percentage based on reports of the literature, which shows that modifications of semiconductors with copper oxides in percentages higher than 3.0% do not improve the formation of the products [36,37], as will be confirmed in this work further ahead.

The composition of the as-synthetized photocatalysts was investigated by X-ray diffraction (XRD) shown in Fig. 1a. The presence of orthorhombic $BiVO_4$ structure (space group: I112/b (15)) is confirmed by the peaks at 2θ = 28.8°; 28.9°; 55.5°; 55.8°; 69.2°; 78.6°, that are related to the planes (013), (−112), (031), (−215), (−118) and, (−235), respectively, according to the Crystmet database (crystallographic card ID876592). An enlargement of the diffraction peaks related to $BiVO_4$ shows that the lamellar structures were obtained for all the photocatalysts [4,25]. The presence of bismuth oxide (Bi_2O_3, space group: P21/c (14)) was observed in the peaks at 2θ = 33.3° and 46.4° related to the planes (200) and (041), respectively, according to the crystallographic card ID140103 (Crystmet database). This secondary semiconductor is commonly observed in the synthesis of $BiVO_4$ powder [4,24,38] and it is a semiconductor with good photoconductivity characteristics [39]. The peak relative to copper oxides that should be observed around 2θ = 35°, 36° or 38° (Crystmet database ID519027 and ID38808), or even to metallic copper (2θ = 43°) (Crystmet database ID26490) is not present in any of the photocatalysts synthesized, probably due to its low concentration and high distribution.

It is interesting to observe that the addition of copper increased the crystallite size, as observed in Table 1. The crystallite sizes of all samples were determined by calculating the XRD peak widths for the Bi_2O_3 peaks corresponding to the [200] and [104] planes (2θ = 33° and 48°, respectively) as shown in Fig. 1a, using the Scherrer equation (Eq. (1)):

$$D_{Sch} = K\lambda/\beta_{hkl}\cos(\theta) \quad (7)$$

Where DSch is the crystallite size, K is a constant equal to 0.9 for the spherical morphology, λ is the XRD incidence wavelength of Cu-kα radiation (0.154 nm), βhkl is the half-width of the peak and θ is the (h k l) peak position [40,41]. It may indicate that the copper has been inserted into the crystal lattice of the photocatalyst during the synthesis by microwave. Once the diameter of Bi^{3+} ions (0.108 nm) [42] is higher than the diameter of Cu^{+} or Cu^{2+} (0.096 and 0.072 nm, respectively) [43] and, the insertion of copper did not decrease, on the contrary, it increased the crystallite size, it is easy to conclude that the modification was not substitutional, but rather interstitial.

The Raman spectra presented in Fig. 1b exhibit vibrational modes that are characteristic of $BiVO_4$ materials. These include an external mode at around 200 cm^{-1}; asymmetric (~325 cm^{-1}) and symmetric (~360 cm^{-1}) VO_4^{-3} bending [44,45]. Additionally, a pronounced band around 810 cm^{-1} is assigned to an A_g mode, which corresponds to the symmetric stretching of the V–O bond [46]. Hardcastle et al. [47] demonstrated that this A_g mode can be employed to estimate the V-O bond length, which in our case increased from ~ 1.705 to ~ 1.706 Å after copper insertion following the same trend observed in the crystallite size (Table 1). The insertion of copper oxide also increased the average crystallite size of TiO_2 and improved the stability of the catalyst for CO_2 reduction, as reported by Torres and coworkers [48]. As the radius of Cu^{+} (0.96 Å) or Cu^{+2} (0.72 Å) is smaller than that of Bi^{+3} (1.08 Å) [42,43], the doping process may occur in interstitial sites [49], expanding the unit cell, reinforcing the results obtained in XRD. Furthermore, the copper doping inserts intermediates electronic levels, which generates an internal electric field that distorts the VO_4^{-3} tetrahedron, causing the observed V-O bond elongation. This phenomenon is of particular interest for the processes involving metal-doped $BiVO_4$-based materials due to the possibility of achieving better photocatalytic performance [50].

SEM images of the photocatalyst with and without the presence of copper oxide can be observed in Fig. 2. The top view of the $BiVO_4$-Bi_2O_3 powder photocatalyst synthesized without the copper precursor presence (Fig. 2a) and with different percentages of copper (Fig. 2b and c) are very similar, indicating the obtaining of a lamellar-shape $BiVO_4$-Bi_2O_3 semiconductor [26]. The copper oxide is present in such low concentration, small size, and highly dispersed that it was not observed

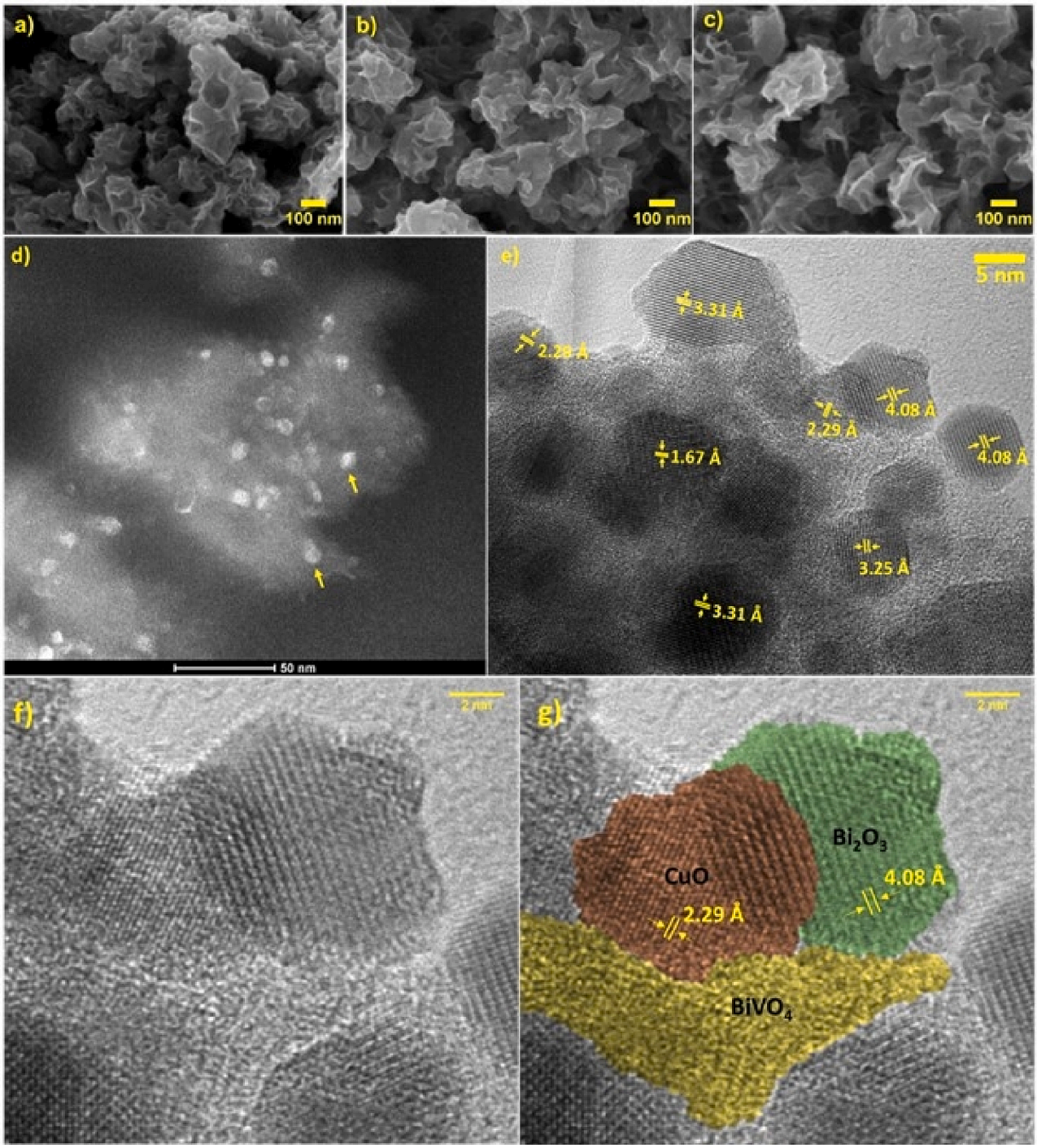

Fig. 2. SEM images of lamellar $BiVO_4$ catalyst a) without copper and with b) 1 %Cu and, c) 2.5 %Cu and d) to g) TEM images of the $BiVO_4$-Bi_2O_3/CuO (1.0%).

in SEM images. However, Fig. 2d reports a high-resolution TEM image of the $BiVO_4$-Bi_2O_3/CuO catalyst evidencing the presence of crystalline structures around 5.0 nm on the lamellar $BiVO_4$-Bi_2O_3 which can be associated with copper oxide nanoparticles. It is also possible to observe in Fig. 2e the existence of different plane and lattice spacing, where the synthesis of CuO and Bi_2O_3 can be proved, once both semiconductors are synthesized with good crystallinity, differently of the lamellar $BiVO_4$ structures, which present low crystallinity. The presence of CuO with lattice spacing measured as 2.29 Å is related to the plane (1 1 1) (Crystmet database ID519027) while the distance of 4.08, 3.31, 3.25, and 1.67 Å are related to the plane (0 2 0), (1 1 1), (1 2 0), and (−2 4 1) of Bi_2O_3 (Crystmet database ID140103). In Fig. 2f and g, it is possible to see the closest approximation of the catalyst with the heterojunction of $BiVO_4$, Bi_2O_3, and CuO highlighted in Fig. 2g. The border of CuO and Bi_2O_3 was defined based on the lattice spacing of each semiconductor, related to the plane (1 1 1) and the plane (0 2 0), respectively. In the case of lamellar $BiVO_4$, once it has low crystallinity, it was based on the literature [26,51].

Fig. 3 presents EDS spectra and elemental mapping analysis for $BiVO_4$-Bi_2O_3/CuO(2.5%) powder catalyst. Analogous results were obtained for the $BiVO_4$-Bi_2O_3 modified with different copper percentages. Copper presence was confirmed by both analyses. The EDS indicates just the presence of the elements Bi, V, O, and Cu, as expected (Fig. 3a). The mapping of chemical elemental obtained using EDS shows a uniform

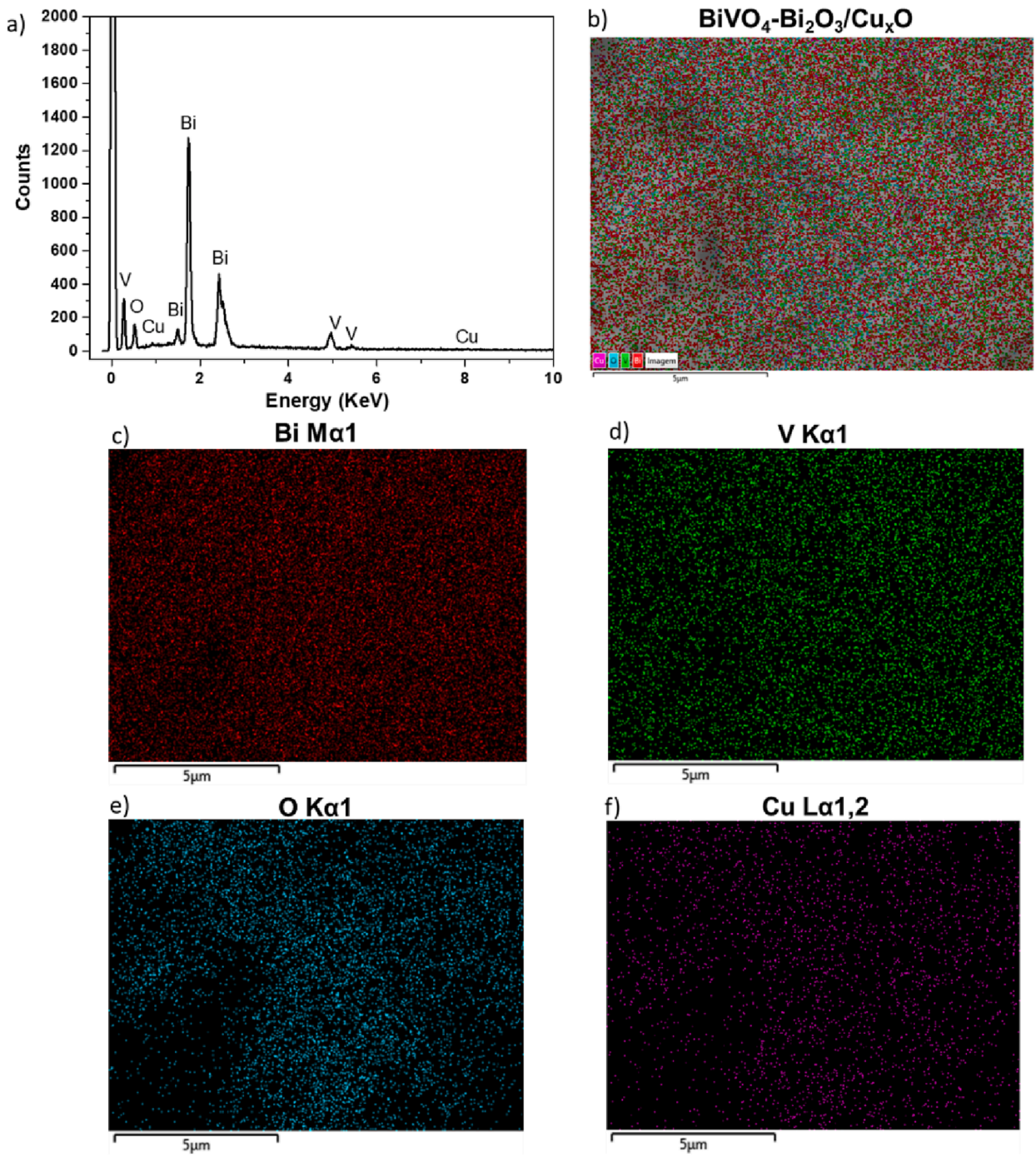

Fig. 3. A) EDS analysis and b–f) elemental mapping analysis of each element present in the bivo$_4$-Bi$_2$O$_3$/CuO photocatalyst.

distribution of Bi, V, O, and Cu, atoms throughout the entire surface.

The high-resolution XPS for $BiVO_4$-Bi_2O_3/Cu is presented in Fig. 4. In the Bi 4*f* spectrum region (Fig. 4a) is observed two pairs of peaks: at 157.8 – 163.1 eV and 158.4–163.7 eV. The first pair corresponds to the Bi $4f_{7/2}$ and Bi $4f_{5/2}$ binding energies (BE) of monoclinic $BiVO_4$, while the second pair refers to Bi_2O_3 [52]. The doublet peaks located at BE about 515.8 and 523.3 eV (Fig. 4b), corresponding to V $2p_{3/2}$ and V $2p_{1/2}$, respectively, referring to V^{5+} cations in the crystal lattice of monoclinic $BiVO_4$ [52,53]. The O 1 *s* region (Fig. 4c) presents three different components. The peaks located at 528.8 eV and 530.3 eV are attributed to O^{2-} at the lattice sites of $BiVO_4$, Bi_2O_3, and CuO species (O_{Lat}) and oxygen-vacancy regions (O_{Vac}), respectively [54,55]. The peak at 532.5 eV is assigned to chemisorbed oxygen and water (O_{ad}) [54]. It is possible to confirm the presence of copper in the material (Fig. 4d), but due to its low concentration, little can be said about its oxidation state. Studies carried out to obtain copper materials in ethyl glycol indicate that the oxidation state of copper on the surface of these samples was dominated by Cu^{2+} [55]. It reinforces the data obtained on TEM images (Fig. 2d and e) where the lattice spacing measures indicated the presence of just CuO, so, the material will be discussed here as $BiVO_4$-Bi_2O_3/CuO.

Catalysts with lamellar structures present high crystallinity and ultrathin thickness [56], benefiting the photocatalytic activity of semiconductors [57]. It may affect positively the $BiVO_4$-Bi_2O_3 photocatalyst activity mainly with the insertion of a cocatalyst such as copper, a well-known material with great properties for CO_2 reduction [58–62]. The behavior of the as-prepared samples under UV–Vis light irradiation was

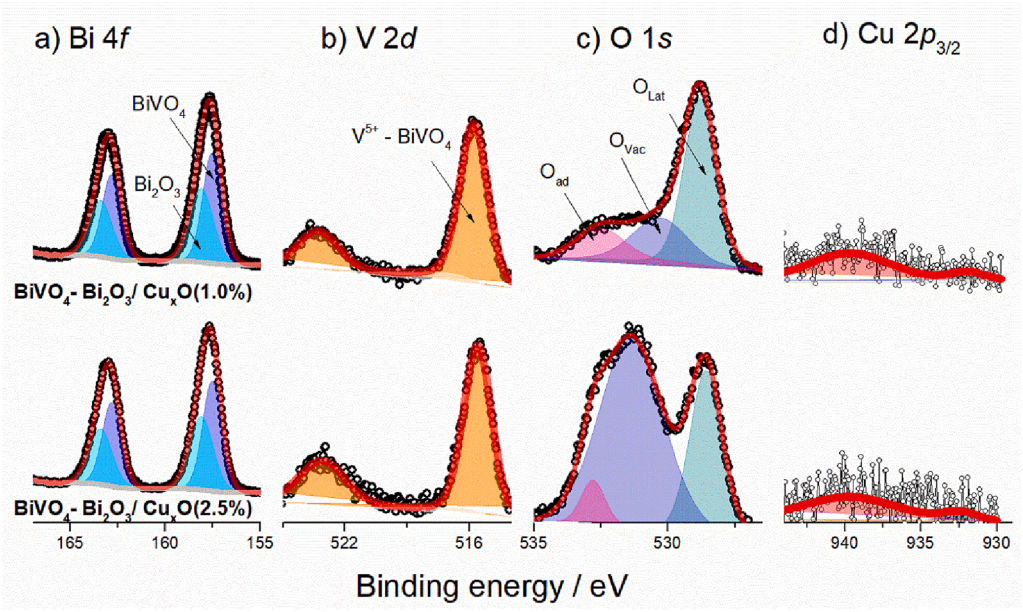

Fig. 4. XPS profile for the $BiVO_4$-Bi_2O_3 photocatalysts with 1.0 and 2.5 of Cu addition on a) Bi 4*f*, b) V 2*d*, c) O 1 *s*, and d) Cu $2p_{3/2}$ orbital regions.

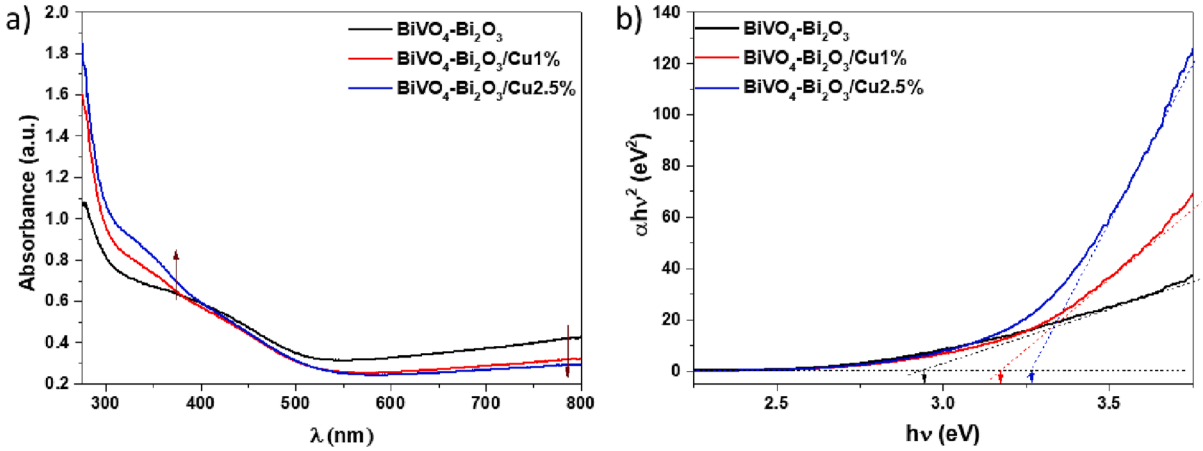

Fig. 5. A) DRS analysis in the UV–Vis region for $BiVO_4$-Bi_2O_3 (black curve) and $BiVO_4$-Bi_2O_3 modified with 1.0% and 2.5% of copper (red and blue curves, respectively) and b) Tauc plot for determination of the band gap in all causes, considering the direct electronic transition.

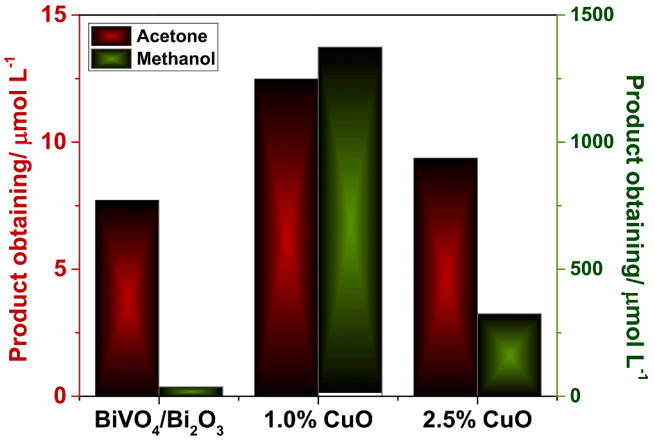

Fig. 6. Acetone and methanol production from CO_2 reduction by photocatalysis technique under $NaHCO_3$ pH 8 using $BiVO_4$ and Cu-$BiVO_4$ photocatalysts with 1.0 and 2.5 of copper.

evaluated by DRS analysis (Fig. 5a), showing that the absorption of light at $BiVO_4$-Bi_2O_3 presents a redshift in the UV region when modified with copper. On the other hand, in the visible region, there is a decrease in the intensity of absorption with modification of the $BiVO_4$-Bi_2O_3. The influence of the copper insertion in the absorption of the lamellar $BiVO_4$-Bi_2O_3 photocatalyst indicates that the copper is present as an oxide phase, once the insertion of a metal does not influence the light absorption or the band gap of a semiconductor [63–65].

The Tauc plot obtained using the Kubelka-Munk function from diffuse reflectance (DRS) spectra for all as-synthesized materials is presented in Fig. 5b. $BiVO_4$ photocatalyst has a direct permissible electronic transition between the bands [4] with a band gap that can vary from 2.4 eV to 3.0 eV [25,66]. The presence of copper oxide changes the light absorption of the photocatalyst and consequently, the band gap value (Fig. 5b). Table 1 presents the band gap values for all as-synthesized samples showing that, as observed in DRS results, the band gap of the $BiVO_4$-Bi_2O_3 photocatalyst had a slight increase with the insertion of CuO, due to an increase in the UV region absorption and a decrease in the visible region absorption, though the percentage of copper had little influence in the band gap value of $BiVO_4$-Bi_2O_3/CuO.

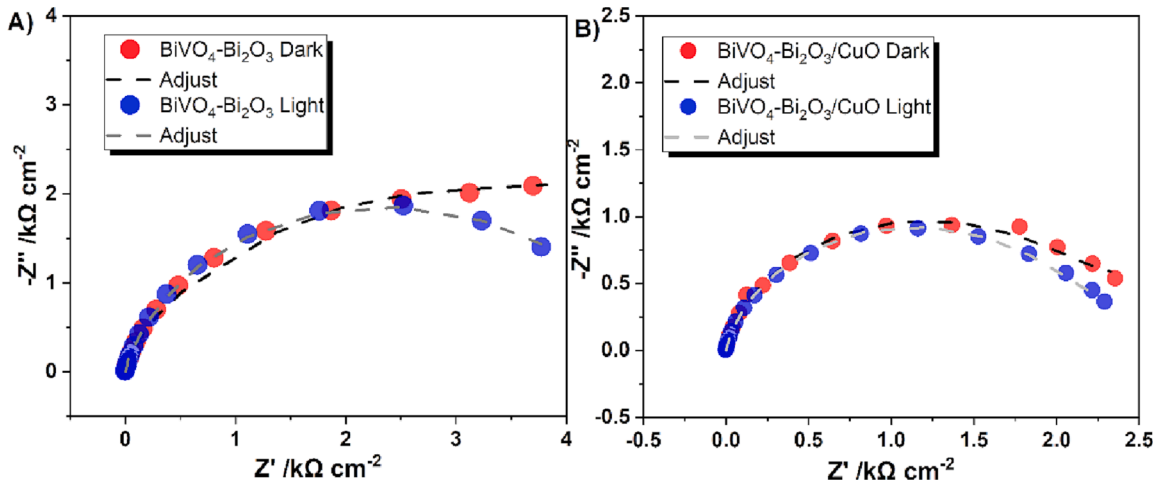

Fig. 7. EIS spectra without (red dots) and under (blue dots) illumination of a) $BiVO_4$-Bi_2O_3, and b) $BiVO_4$-Bi_2O_3/CuO photocatalyst.

The same behavior was already observed in the literature for the junction of copper oxides and other main semiconductors [48,67]. An increase in the band gap value of CuO while the percentage of CuO is incorporated in a composite was also reported [68]. The rational design of semiconductors goes beyond the bandgap, it involves also the band edge positions and the surface CO_2 adsorption capacity [69], and both aspects were improved with the CuO presence on the $BiVO_4$-Bi_2O_3 photocatalyst, as will be demonstrated hereafter.

3.2. Photocatalytic reduction of CO_2 under $BiVO_4$-Bi_2O_3/CuO

The influence of the amount of copper on the photoactivity of $BiVO_4$-Bi_2O_3 semiconductor in the CO_2 reduction using the photocatalysis technique was investigated based on the concentration of the products generated after 2 h of photoreaction. The conditions employed for the CO_2 reduction reaction, such as temperature, pH, supporting electrolyte, and time of reaction were chosen based on the literature [13,70,71]. As can be observed in Fig. 6, there are differences just in the concentration of the products generated from the CO_2 reduction according to the Cu amount present in the $BiVO_4$-Bi_2O_3 photocatalyst, the molecules that are formed in all the cases are the same, methanol and acetone. In the case of both products synthesis, amounts of the cocatalyst higher than 1.0 % do not improve the photoactivity of the $BiVO_4$-Bi_2O_3 semiconductor for CO_2 reduction. On the contrary, there was a decrease in the concentration of methanol and acetone formation reaching production values lower than those obtained using $BiVO_4$-Bi_2O_3 semiconductor without further modification, indicating that amounts of copper doping large than 1.0% may create recombination centers, reducing the photocatalytic performance.

The best amount of Cu cocatalyst able to improve the formation of products from the CO_2 reduction was 1.0%, reaching 12.5 μmol L^{-1} g_{cat}^{-1} acetone and 1373.5 μmol L^{-1} g_{cat}^{-1} methanol. The presence of the cocatalyst improved 38 times methanol production and 62% of the acetone amount compared to the photocatalysts without CuO modification [4]. Slamet and coworkers [37] have observed that copper can increase methanol yields up to 3.0% of CuO loading, amounts higher than that can cause shadows in the semiconductor surface reducing its photo-exciting capacity, which is possibly what occurs in the case of 2.5 of CuO loading (Fig. 6). Singhal et al. [72] also observed 1% of Cu loading as the best amount for CO_2 reduction using TiO_2 as a semiconductor, however, in this case, the products obtained were CO and H_2. Under similar synthesis conditions for the obtaining of $BiVO_4$ photocatalyst, the production of methanol does not reach an average value higher than 360.0 μmol L^{-1} g_{cat}^{-1} for 2 h of reduction reaction in the same experimental condition as the employed in the present work [4]. It shows the improvement already obtained from the junction of both semiconductors, $BiVO_4$ and Bi_2O_3. However, the metallic cocatalyst shows to be essential to enhance methanol and acetone production from the reduction of CO_2.

To achieve higher efficiency in photochemical redox reactions it is necessary to take full advantage of the charge carriers photogenerated in the catalyst and its interface with the electrolyte [73]. For that, it is necessary to optimize the electronic structure and, to align the band positions of the semiconductors between each of them and between the reduction reaction, due to the strong dependence of the reaction effectivity on the charge transfer process [74].

As discussed in companion work [4,26], the CO_2 reduction by photocatalysis technique under $BiVO_4$-based photocatalysts occurs initially by the photoactivation of the semiconductors by the incidence of photons with enough energy to photoexcite the electrons through the band gap to reach the conduction band (CB), generating holes in the absence of the electron at the valence band (VB). This is a simple mechanism for photoactivation of semiconductors by light incidence, and like many, there is the problem of charge recombination which can delay the CO_2 reduction process. It can be polished up by the combination of two semiconductors, with the electrons and holes being driven to the semiconductor with lower CB and VB energy [71,75].

The first step for the formation of fuels through the CO_2 reduction by photocatalysis technique happens with the transfer of one electron from the photocatalyst surface to the CO_2 molecule adsorbed in this photocatalyst surface, generating the radical $^{-}CO_2$ [76,77], as demonstrated in Eq. (4). After that, the products are formed by successive reactions of protons (H^+) and electrons (e^-) [71,75]. Concerning the products obtained in the present work, it is necessary 6 H^+ and 6 e^- to convert 1 molecule of CO_2 into methanol, while for acetone is necessary 16 H^+ and 16 e^- [78,79].

3.3. Photochemical characterization of $BiVO_4$-Bi_2O_3/CuO

As explored above, the sample containing 1.0% showed the best photocatalytic performance among the evaluated samples. Aiming to investigate this difference, EIS was performed and is presented in Fig. 7. The results were adjusted using a Randles equivalent circuit. Due to the presence of ethyl cellulose, employed in the deposition process, the samples showed relatively high resistive behavior (in the order of kΩ), and small differences between light and dark conditions of measurement. Unmodified $BiVO_4$-Bi_2O_3 presented a charge transfer resistance (R_{ct}) of 4.54 and 3.38 kΩ under dark and light respectively (Fig. 7a), on the other way, the sample with 1.0% of copper ($BiVO_4$-Bi_2O_3/CuO) showed a noteworthy reduction of R_{ct}, being 2.21 and 2.16 kΩ (under dark and light, Fig. 7b). Despite the resistance due to the presence of ethyl cellulose, this reduction of R_{ct} shows how the presence of CuO can

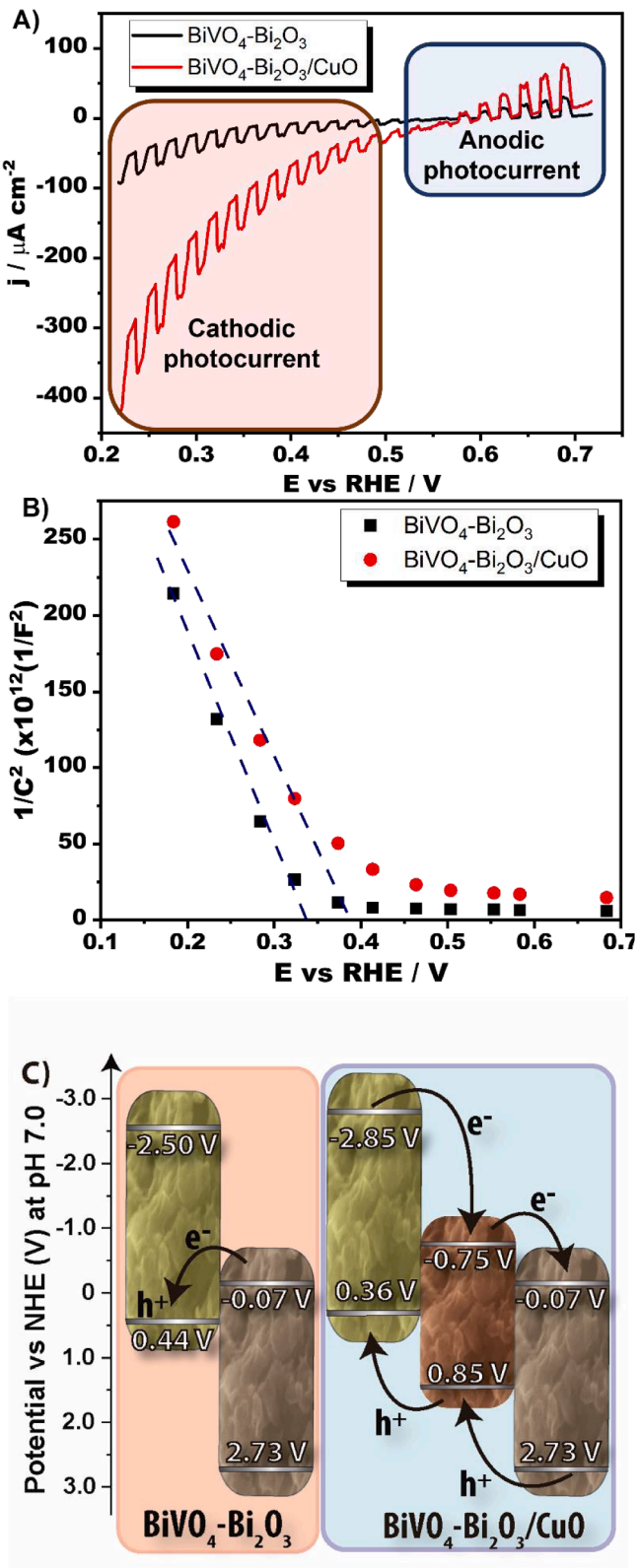

Fig. 8. a) Transient photocurrent, b) Mott- Schottky obtained for the pure $BiVO_4$-Bi_2O_3 (black) and $BiVO_4$-Bi_2O_3/CuO (red) samples, in Na_2SO_4 0.5 mol L^{-1}, pH 8.5 under N_2 atmosphere, and **c)** Band position of the samples $BiVO_4$-Bi_2O_3 (salmon) and $BiVO_4$-Bi_2O_3/CuO (blue).

improve the transfer of photogenerated charges, which can further provide the electrons for CO_2 reduction. It reinforces the results obtained in photocatalysis, as long the better charge transfer leads to mitigation of the charge recombination process and, consequently improves the products (acetone and methanol) yield.

The influence of the charge transfer process observed in EIS measurement could also be observed in the photocurrent measurements, shown in Fig. 8a. Employing ethyl cellulose hinders the obtained photocurrent, leading to values less than 100 μA cm^{-2}. However, is noteworthy that the photocurrent for the $BiVO_4$-Bi_2O_3/CuO reached values much higher than for the unmodified sample, indicative of the better charge transfer due to CuO presence [42]. In the graph is possible to observe two distinct regions, the first under ~ 0.5 V vs RHE where both $BiVO_4$-Bi_2O_3 and $BiVO_4$-Bi_2O_3/CuO presented cathodic photocurrent, in agreement with the p-type nature observed for the materials, with values more than two times higher after copper addition (70 and 30 μA cm^{-2} at 0.3 V vs RHE for $BiVO_4$-Bi_2O_3/CuO and $BiVO_4$-Bi_2O_3 respectively). The region above ~ 0.5 V vs RHE shows an inversion of the photocurrent, which indicates that the electron transfer process changed from being mediated by the CB to the VB due to the applied bias.

According to the literature, the flat band potential (E_{FB}) must be located in the potential where the photocurrent inversion occurs, being estimated at ~ 0.55 V vs RHE for both samples. In addition, for materials with p-type behavior, the E_{FB} is located at about 0.1 V near the VB edge [80–82]. However, due to the low photocurrent values in this inversion range, this technique is not the most precise for E_{FB} determination. Furthermore, the cathodic photocurrent was more noticeable than the anodic, reinforcing again the p-type attributes from the samples. This fact brings to light that, with a deep optimization of the photoelectrode fabrication (e. g. deposition process, electric contact, etc), aiming to improve the photocurrent response, the hereby reported material is a promising candidate for applications such as overall water splitting.

Aiming for a better comprehension of the E_{FB}, Mott-Schottky measurements were conducted (Fig. 8b), both samples exhibited a characteristic nature of p-type semiconductors, as can be observed in the negative slope of the plot [81,82]. The E_{FB} was determined from the extrapolation of the tangent line of the plot to the x-axis, the values found were 0.41 and 0.33 V vs RHE for the samples without and with CuO respectively These values are near the VB edge expected from photocurrent measurements (~0.1 V above E_{FB}). Also, according to the Mott-Schottky equation [83], the decrease in the slope of the plot indicates qualitatively an increase in the free carrier concentration in the material, common from the doping process, and that reinforces better photocatalytic activity [84].

From the Mott-Schottky analysis, we were able to build a band diagram for the samples, as represented in Fig. 8c. Considering the epitaxial growth of bismuth oxide, the CB edge position of Bi_2O_3 [85] is much closer to the VB edge of $BiVO_4$, which can induce quenching of the photogenerated charge carriers in the sample, thereby reducing the photocatalytic activity. On the other hand, due to the intermediary value of CuO bands [1], it favors band bending in the interface between the semiconductors, which improves charge separation. In this sense, the better performance observed for CO_2 reduction in the sample containing CuO can be attributed to three main factors: i) the catalytic properties of copper for adsorption and activation of CO_2 for further conversion; ii) the band position of the synthesized $BiVO_4$ with energy enough to perform more complex reactions such as obtaining C3 molecules like acetone ($E^0 = -0.61$ V vs NHE) and; iii) better charge separation in the architecture $BiVO_4$-Bi_2O_3/CuO due the favorable band position of the semiconductors.

4. Conclusion

The design of the lamellar $BiVO_4$-based catalyst drove it to a p-type condition, which is essential for its application in the CO_2

photoreduction process. The temperature employed in the microwave method culminated in the co-formation of Bi_2O_3, generating a heterostructure. The modification of the lamellar $BiVO_4$-Bi_2O_3 with CuO changed the light absorption and, consequently, the band gap, decreased the resistance and the flat band potential, improved the photocurrent density and also, the methanol and acetone production compared with the $BiVO_4$-Bi_2O_3 photocatalyst. Small amounts of copper oxide showed to be the best choice to increment the CO_2 conversion to organic fuels. The insertion of 1.0% of copper in the microwave synthesis resulted in an increase of 38 times for methanol generation and 62% for the acetone formation after 4 h of photoreduction of CO_2 under ambient conditions compared to the photocatalyst without copper. Linear sweep voltammetry under transient light incidence and Mott-Schottky measurements showed a higher conduction band position for the $BiVO_4$-Bi_2O_3/CuO semiconductor which naturally favors the photocatalytic reduction process, at the same time that the valence band showed a lower value, improving the water oxidation, necessary to generates the protons used to methanol and acetone production. This deep optimization of the photocatalyst fabrication drove a well-designed semiconductor for CO_2 reduction under just light incidence generating high concentrations of energetic compounds.

CRediT authorship contribution statement

Patricia Gon Corradini: Writing – review & editing, Writing – original draft, Methodology, Investigation, Data curation. **Juliana Ferreira de Brito:** Writing – review & editing, Writing – original draft, Visualization, Investigation. **Sirlon F. Blaskievicz:** Writing – review & editing, Writing – original draft, Investigation, Data curation. **Byanca S. Salvati:** Writing – review & editing, Data curation. **Beatriz Costa e Silva Menezes:** Data curation, Writing – review & editing. **Maria Valnice Boldrin Zanoni:** Visualization, Writing – review & editing, Resources. **Lucia Helena Mascaro:** Visualization, Supervision, Writing – review & editing, Resources.

Declaration of Competing Interest

The authors declare the following financial interests/personal relationships which may be considered as potential competing interests: Lucia Helena Mascaro reports financial support was provided by State of Sao Paulo Research Foundation. Juliana Ferreira de Brito reports financial support was provided by State of Sao Paulo Research Foundation. Sirlon F. Blaskievicz reports financial support was provided by National Council for Scientific and Technological Development. Lucia Helena Mascaro reports financial support was provided by Financiadora de Estudos e Projetos (FINEP). Maria Valnice Boldrin Zanoni reports financial support was provided by INCT-DATREM. Lucia Helena Mascaro reports financial support was provided by Shell. Lucia Helena Mascaro reports financial support was provided by National Agency of Oil Natural Gas and Biofuels. Lucia Helena Mascaro reports equipment, drugs, or supplies was provided by LCE, DEMa, UFSCar.

Data availability

Data will be made available on request.

Acknowledgments

Funding: This work was supported by: São Paulo Research Foundation, FAPESP [grant numbers #2018/02950-0, #2018/16401-8, #2013/07296-2, and #2017/11986-5], Coordenação de Aperfeiçoamento de Pessoal de Nível Superior - Brazil, CAPES [grant number 001], Conselho Nacional de Pesquisa e Desenvolvimento, CNPq, [grant numbers #152607/2022-6, #311769/2022-5 and #406156/2022-0] and INCT-DATREM [grant number #465571/2014-0]. The authors thank Shell and the strategic importance of the support given by ANP (Brazil's National Oil, Natural Gas, and Biofuels Agency) through the R&D levy regulation, and the Laboratory of Structural Characterization, LCE/DEMa/UFSCar, for the general facilities.

References

[1] S.C. Roy, O.K. Varghese, M. Paulose, C.A. Grimes, ACS Nano 4 (2010) 1259–1278.
[2] G.G. Bessegato, T.T. Guaraldo, J.F. de Brito, M.F. Brugnera, M.V.B. Zanoni, Electrocatalysis 6 (2015) 415–441.
[3] J.F. de Brito, P.G. Corradini, A.B. Silva, L.H. Mascaro, ChemElectroChem 8 (2021) 4305–4320.
[4] P.G. Corradini, J.F. De Brito, M.V.B. Zanoni, L.H. Mascaro, J. CO2 Util. 36 (2020) 187–195.
[5] U. Kang, S.K. Choi, D.J. Ham, S.M. Ji, W. Choi, D.S. Han, A. Abdel-Wahab, H. Park, Energy Environ. Sci. (2015) 2638.
[6] D. Won, J. Lee, Q. Ba, Y. Cho, H. Cheong, S. Choi, C.H. Kim, H. Son, C. Pac, S. O. Kang, ACS Catal. 8 (2018) 1018–1030.
[7] Q. Xie, W. He, S. Liu, C. Li, J. Zhang, P.K. Wong, Chin. J. Catal. 41 (2020) 140–153.
[8] A.E. Nogueira, J.A. Oliveira, G.T.S.T. Silva, C. Ribeiro, Sci. Rep. 9 (2019) 1–11.
[9] J.F. de Brito, F. Tavella, C. Genovese, C. Ampelli, M.V.B. Zanoni, G. Centi, S. Perathoner, Appl. Catal. B Environ. 224 (2018) 136–145.
[10] K. Rajeshwar, J. Phys. Chem. 2 (2011) 1301–1309.
[11] K. Rajeshwar, A. Thomas, C. Janaky, J. Phys. Chem. Lett. 6 (2015) 139–147.
[12] J.F. Brito, A.A. Silva, A.J. Cavalheiro, M.V.B. Zanoni, Int. J. Electrochem. Sci. 9 (2014) 5961–5973.
[13] J.F. Brito, A.R. Araujo, K. Rajeshwar, M.V.B. Zanoni, Chem. Eng. J. 264 (2015) 302–309.
[14] J. Yuan, X. Wang, C. Gu, J. Sun, W. Ding, J. Wei, X. Zuo, C. Hao, RSC Adv. 7 (2017) 24933–24939.
[15] P. Li, J. Xu, H. Jing, C. Wu, H. Peng, J. Lu, H. Yin, Appl. Catal. B Environ. 156–157 (2014) 134–140.
[16] M.L. Ovcharov, A.M. Mishura, N.D. Shcherban, S.M. Filonenko, V.M. Granchak, Sol. Energy 139 (2016) 452–457.
[17] K.C. Christoforidis, P. Fornasiero, ChemCatChem 11 (2019) 368–382.
[18] Y. Yang, S. Ajmal, X. Zheng, L. Zhang, Sustain. Energy Fuels 2 (2018) 510–537.
[19] X. Liu, J. Xiao, H. Peng, X. Hong, K. Chan, Nat. Commun. 8 (2017) 1–7.
[20] Z. Zhang, P. Wang, J. Mater. Chem. 22 (2012) 2456.
[21] P. Li, J. Zhang, H. Wang, H. Jing, J. Xu, X. Sui, H. Hu, H. Yin, Catal. Sci. Technol. 4 (2014) 1070.
[22] T.T. Guaraldo, J.F. de Brito, D. Wood, M.V.B. Zanoni, Electrochim. Acta 185 (2015) 117–124.
[23] L.H. Mascaro, A. Pockett, J.M. Mitchels, L.M. Peter, P.J. Cameron, V. Celorrio, D. J. Fermin, J.S. Sagu, K.G.U. Wijayantha, G. Kociok-Köhn, F. Marken, J. Solid State Electrochem. 19 (2014) 31–35.
[24] L. Chen, Q. Zhang, R. Huang, S.F. Yin, S.L. Luo, C.T. Au, Dalt. Trans. 41 (2012) 9513–9518.
[25] S. Gao, B. Gu, X. Jiao, Y. Sun, X. Zu, F. Yang, W. Zhu, C. Wang, Z. Feng, B. Ye, Y. Xie, J. Am. Chem. Soc. 139 (2017) 3438–3445.
[26] J.F. de Brito, P.G. Corradini, M.V.B. Zanoni, F. Marken, L.H. Mascaro, J. Alloys Compd. 851 (2021) 156912.
[27] S. Chen, D. Huang, P. Xu, X. Gong, W. Xue, L. Lei, R. Deng, J. Li, Z. Li, ACS Catal. 10 (2020) 1024–1059.
[28] H. Wang, R. Hailili, X. Jiang, G. Yuan, D.W. Bahnemann, X. Wang, Nanotechnology (2023) 34, https://doi.org/10.1088/1361-6528/acbb7c.
[29] J. Mao, T. Peng, X. Zhang, K. Li, L. Zan, Catal. Commun. 28 (2012) 38–41.
[30] Y. Zhang, L. Zheng, J. Jia, K. Li, T. Zhang, H. Yu, Colloids Surf. A Physicochem. Eng. Asp. 639 (2022) 128321.
[31] L. Chen, J. Wang, D. Meng, Y. Xing, C. Wang, F. Li, Y. Wang, X. Wu, Mater. Lett. 147 (2015) 1–3.
[32] L. Li, B. Yan, J. Alloys Compd. 476 (2009) 624–628.
[33] A.B. Cezar, I.L. Graff, J. Varalda, W.H. Schreiner, D.H. Mosca, J. Appl. Phys. 116 (2014), https://doi.org/10.1063/1.4899249.
[34] A. Dolgonos, T.O. Mason, R. Kenneth, J. Solid State Chem. 240 (2016) 43–48.
[35] J.F. de Brito, J.A.L. Perini, S. Perathoner, M.V.B. Zanoni, Electrochim. Acta 306 (2019) 277–284.
[36] S. Qin, F. Xin, Y. Liu, X. Yin, W. Ma, J. Colloid Interface Sci. 356 (2011) 257–261.
[37] Slamet, H.W. Nasution, E. Purnama, S. Kosela, J. Gunlazuardi, Catal. Commun. 6 (2005) 313–319.
[38] P. Qiu, B. Park, J. Choi, M. Cui, J. Kim, J. Khim, J. Alloys Compd. 706 (2017) 7–15.
[39] I.N. Reddy, C.V. Reddy, A. Sreedhar, M. Cho, D. Kim, J. Shim, Ceram. Int. 45 (2019) 16784–16791.
[40] J. Madhavi, SN Appl. Sci. 1 (2019) 1–12.
[41] B. Lei, L. Zeng, P. Zhang, Z. Sun, W. Sun, X. Zhang, Adv. Powder Technol. 25 (2014) 946–951.
[42] C. Liu, X. Li, J. Su, L. Guo, Int. J. Hydrogen Energy 41 (2016) 12842–12851.
[43] M. Wang, F. Ren, G. Cai, Y. Liu, S. Shen, L. Guo, Nano Res. 7 (2014) 353–364.
[44] D. Wang, H. Jiang, X. Zong, Q. Xu, Y. Ma, G. Li, C. Li, Chem. - A Eur. J. 17 (2011) 1275–1282.
[45] Y. Xue, X. Wang, Int. J. Hydrogen Energy 40 (2015) 5878–5888.
[46] F.W.P. Ribeiro, M.F. Gromboni, F. Marken, L.H. Mascaro, Int. J. Hydrogen Energy 41 (2016) 1–10.
[47] F.D. Hardcastle, I.E. Wachs, J. Phys. Chem. 95 (1991) 5031–5041.

[48] J.A. Torres, J.C. da Cruz, A.E. Nogueira, G.T.S.T. da Silva, J.A. de Oliveira, C. Ribeiro, J. Environ. Chem. Eng. (2022) 10, https://doi.org/10.1016/j.jece.2022.107291.
[49] S. Peng, Y. Li, F. Jiang, G. Lu, S. Li, Chem. Phys. Lett. 398 (2004) 235–239.
[50] H.S. Park, K.E. Kweon, H. Ye, E. Paek, G.S. Hwang, A.J. Bard, J. Phys. Chem. C 115 (2011) 17870–17879.
[51] K.R. Tolod, S. Hernández, N. Russo, Catalysts (2017) 7, https://doi.org/10.3390/catal7010013.
[52] Y. Bi, Y. Yang, X.L. Shi, L. Feng, X. Hou, X. Ye, L. Zhang, G. Suo, J. Chen, Z.G. Chen, J. Colloid Interface Sci. 593 (2021) 196–203.
[53] J. Ge, X. Ding, D. Jiang, L. Zhang, P. Du, Catal. Lett. 151 (2021) 1231–1238.
[54] J.M. Wu, Y. Chen, L. Pan, P. Wang, Y. Cui, D.C. Kong, L. Wang, X. Zhang, J.J. Zou, Appl. Catal. B Environ. 221 (2018) 187–195.
[55] L. Xu, Y. Yang, Z.W. Hu, S.H. Yu, ACS Nano 10 (2016) 3823–3834.
[56] M. Shang, W. Wang, L. Zhang, J. Hazard. Mater. 167 (2009) 803–809.
[57] L. Su, L. Luo, H. Song, Z. Wu, W. Tu, Z. jun Wang, J. Ye, Chem. Eng. J. 388 (2020) 124346.
[58] J.F. Brito, C. Genovese, F. Tavella, C. Ampelli, M.V.B. Zanoni, G. Centi, S. Perathoner, ChemSusChem 12 (2019) 4274–4284.
[59] I. Ganesh, P.P. Kumar, I. Annapoorna, J.M. Sumliner, M. Ramakrishna, N. Y. Hebalkar, G. Padmanabham, G. Sundararajan, Appl. Surf. Sci. 293 (2014) 229–247.
[60] B.C.E. Silva, K. Irikura, J.B.S. Flor, R.M.M. Dos Santos, A. Lachgar, R.C.G. Frem, M. V.B. Zanoni, J. CO2 Util. 42 (2020) 101299.
[61] J.F. de Brito, K. Irikura, C.M. Terzi, S. Nakagaki, M.V.B. Zanoni, J. CO2 Util. 41 (2020) 101261.
[62] K. Eid, M.H. Sliem, K. Jlassi, A.S. Eldesoky, G.G. Abdo, Inorg. Chem. Commun. 107 (2019) 107460.
[63] C.A.G. Bezerra, J.P.T. da S. Santos, G.G. Bessegato, C.L. de Paiva e Silva Zanta, V. Del Colle, G. Tremiliosi-Filho, Electrochim. Acta 404 (2022), https://doi.org/10.1016/j.electacta.2021.139712.
[64] Q. Shen, Z. Chen, X. Huang, M. Liu, G. Zhao, Environ. Sci. Technol. 49 (2015) 5828–5835.
[65] M.V. de L. Tinoco, M.B. Costa, L.H. Mascaro, J.F. de Brito, Electrochim. Acta 382 (2021) 138290.
[66] L. Zhang, D. Chen, X. Jiao, J. Phys. Chem. B 110 (2006) 2668–2673.
[67] F. Fang, Y. Liu, X. Sun, C. Fu, Y. Prakash Bhoi, W. Xiong, W. Huang, Appl. Surf. Sci. 564 (2021), https://doi.org/10.1016/j.apsusc.2021.150407.
[68] J.D.C. Geovo, J.A. Torres, A.S. Giroto, F.C.N. Rocha, M.M. Garcia, G.T.S.T. Silva, J. R.C. Souza, J.A. de Oliveira, C. Ribeiro, A.E. Nogueira, J. Photochem. Photobiol. A Chem. 439 (2023), https://doi.org/10.1016/j.jphotochem.2023.114631.
[69] P. Wang, S. Wang, P. Wang, S. Wang, H. Wang, Z. Wu, L. Wang, Part. Part. Syst. Charact. 35 (2018) 1–25.
[70] J.F. de Brito, A.A. da Silva, A.J. Cavalheiro, M.V.B. Zanoni, Evaluation of the Parameters Affecting the Photoelectrocatalytic Reduction of CO 2 to CH 3 OH at Cu/Cu 2 O Electrode, 2014.
[71] J.F. de Brito, M.V.B. Zanoni, Chem. Eng. J. 318 (2017) 264–271.
[72] N. Singhal, A. Ali, A. Vorontsov, C. Pendem, U. Kumar, Appl. Catal. A, Gen. 523 (2016) 107–117.
[73] J. Xiong, J. Di, H. Li, J. Mater. Chem. A 8 (2020) 12928–12950.
[74] Y. Zhao, G.I.N. Waterhouse, G. Chen, X. Xiong, L.-Z. Wu, C.-H. Tung, T. Zhang, Chem. Soc. Rev. 48 (2019) 1972–2010.
[75] J.F. de Brito, F.F. Hudari, M.V.B. Zanoni, J. CO2 Util. 24 (2018) 81–88.
[76] N.M. Dimitrijevic, B.K. Vijayan, O.G. Poluektov, T. Rajh, K.a. Gray, H. He, P. Zapol, J. Am. Chem. Soc. 133 (2011) 3964–3971.
[77] J. de Almeida, M.S. Pacheco, J.F. de Brito, C. de Arruda Rodrigues, J. Solid State Electrochem. 24 (2020) 3013–3028.
[78] E. Kecsenovity, B. Endrődi, P.S. Tóth, Y. Zou, R.A.W. Dryfe, K. Rajeshwar, C. Janáky, J. Am. Chem. Soc. 139 (2017) 6682–6692.
[79] J.F. Brito, A.R. Araújo, K. Rajeshwar, M.V.B. Zanoni, Chem. Eng. J. 264 (2015) 302–309.
[80] K. Gelderman, L. Lee, S.W. Donne, J. Chem. Educ. 84 (2007) 685.
[81] D. Xiong, Q. Zhang, S.K. Verma, X.Q. Bao, H. Li, X. Zhao, Mater. Res. Bull. 83 (2016) 141–147.
[82] K. Fujii, K. Ohkawa, Japanese J. Appl. Phys., Part 2 Lett. 44 (2005) 2–5.
[83] S.N.S. Nasir, N.A. Mohamed, M.A. Tukimon, M.F.M. Noh, N.A. Arzaee, M.A. M. Teridi, Phys. B Condens. Matter 604 (2021) 412719.
[84] M.C.K. Sellers, E.G. Seebauer, Thin Solid Films 519 (2011) 2103–2110.
[85] Z. Grubač, J. Katić, M. Metikoš-Huković, J. Electrochem. Soc. 166 (2019) H433–H437.